MONTE CARLO STUDIES ON ELONGATION OF LIQUID CRYSTAL ELASTOMERS UNDER EXTERNAL ELECTRIC FIELD

E. V. Proutorov[1], H. Koibuchi[2]

[1]Department of Physics, Cherepovets State University,
Lunacharsky Prospect 5, Cherepovets 162600, Russia

[2]National Institute of Technology, Ibaraki College,
Nakane 866, Hitachinaka, Ibaraki 312-8508, Japan

Abstract

We study the elongation of three–dimensional (3D) liquid crystal elastomers (LCE) under external electric field by using Finsler Geometry model. The interaction between liquid crystals (LC) and polymer (or bulk material) is implemented in the Finsler metric. For describing directional degrees of LC molecules, we use variable σ. Performing Monte Carlo simulation for 3D LCE object, we find that the strain versus electric field is in good agreement with reported experimental data.

Key words: *liquid crystal elastomers, Monte Carlo, Finsler geometry, external electric field*

1. INTRODUCTION

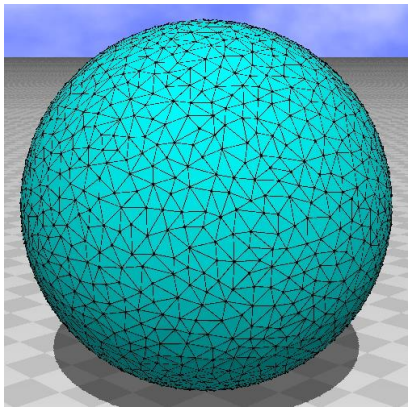
LCE is a flexible material composed of polymeric elastomers and liquid crystal (LC) molecules and attracts a lot of attention in engineering applications. There are several reviews and books for LCE (Ohm, Brehmer and Zentel 2010; Sánchez-Ferrer 2014; Urayama 2007; Warner and Terentjev 2003). Their most interesting property is the reversible shape change under applied external filed, and this property is independent of the nature of forces; mechanical force or electric field. This was predicted by de Gennes in 1975 (de Gennes 1975). Since then it has been discussed that LCEs can be used as sensors, actuators, and artificial muscles in robots (de Gennes, Hébert and Kant 1997; Madden et al. 2004).

Reorientation of the LC director in electric fields is the basis for liquid crystal displays. Therefore, this property of LC also plays an important role inside the polymer network of LCE. Thus, the network is reoriented inside LCE, and the LCE shape is changed. However, despite that the properties of the polymers and liquid crystals are well known, the elongation mechanism of LCE is poorly understood. The main difficulty comes from the fact that the shape change originates in the structural change. It is impossible to change the direction of LC molecules if the shape of LCE is kept fixed (Urayama 2011). Therefore, to understand the mechanism for the elongation of LCE, it is necessary to clarify the interaction between the directional degrees of freedom $\vec{\sigma}$ of LC and the positional degrees of freedom $\vec{r}$ of LC in LCE. This interaction is implemented in the Finsler geometry (FG) model. More detailed information is written in (Osari and Koibuchi 2017). In the FG model the interaction energy between $\vec{\sigma}$s is assumed in the Hamiltonian. The responses to the external mechanical forces and thermal fluctuations are clarified (Osari and Koibuchi 2017).

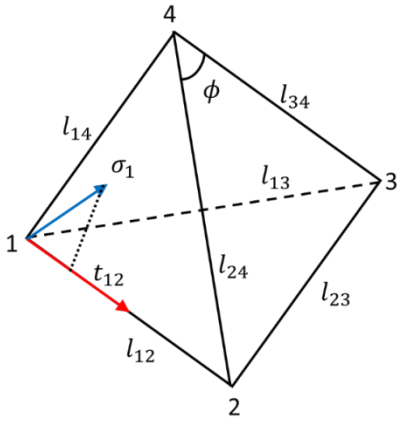
However, the detailed information of the response to the external electric field is not yet obtained. It was reported that this response can be studied by using FG model (Koibuchi 2017). In this paper, we study the elongation of LCE under external electric field using the FG model, with two different Finsler metrics, and we compare the Monte Carlo (MC) simulation results with the reported experimental data.

2. THE MODEL

In this section, we introduce a discrete 3D FG model for 3D LCE. For more detailed information on the 2D FG model please see (Koibuchi and Sekino 2014). The spherical body is constructed by Voronoi tessellation with tetrahedrons, which are composed of vertices, bonds and triangles (Figs.1(a), 1(b)). The mean bond lengths inside sphere are almost the same as the mean bond lengths on the surface. The reason why sphere is used is because the simulations are relatively easy for spheres than for cylinders.



(a)



(b)

Fig. 1. (a) Triangulated spherical body with $N = 10619$, where N is total number of vertices. (b) Tetrahedron on which Hamiltonian is defined, where l_{ij} is the bond length from i to j vertices, t_{12} is the unit vector of the bond between 1 and 2 vertices, σ_1 represents the direction of LC molecule at 1 vertex.

The discrete Hamiltonian $S(\vec{r},\vec{\sigma})$ is defined by:

$$
\begin{aligned}
&S(\bar{r},\bar{\sigma}) = \lambda S_0 + \gamma S_1 + \kappa S_2 + \alpha S_3 + U_{3D}, \quad (\gamma = 1),\\
&S_0(\bar{\sigma}) = \tfrac{1}{2}\textstyle\sum_{ij}\left[1 - 3\left(\vec{\sigma}_i \cdot \vec{\sigma}_j\right)^2\right],\\
&S_1(\vec{r},\vec{\sigma}) = \frac{1}{4\bar{N}}\sum_{ij}\gamma_{ij}l_{ij}^2, \qquad \Gamma_{ij} = \sum_{\text{tet}}\gamma_{ij}(\text{tet}), \qquad l_{ij}^2 = \left(\vec{r}_i - \vec{r}_j\right)^2,\\
&S_2(\vec{r}) = \sum_i [1 - \cos(\phi_i - \pi/3)],\\
&S_3(\vec{\sigma}) = -\sum_i \left(\vec{\sigma}_i \cdot \vec{E}\right)^2, \quad \vec{E} = (E,0,0),\\
&U_{3D} = \sum_{\text{tet}} U_{3D}(\text{tet}), \qquad U_{3D}(\text{tet}) = \begin{cases} 0 & (\text{Vol}(\text{tet}) > 0) \\ \infty & (\text{otherwise}) \end{cases}.
\end{aligned}
\tag{1}
$$

Where $\vec{r}$ and $\vec{\sigma}$ is the three-dimensional vertex position and the directional degrees of freedom of an LC molecule, respectively. λS_0 is the interaction energy between $\vec{\sigma}$s, and the non-polar interaction is assumed between $\vec{\sigma}$s with the interaction strength λ. For $\lambda \to 0$, $\vec{\sigma}$ becomes disordered (corresponding to the isotropic phase) and no anisotropy is expected, while for $\lambda \to \infty$ $\vec{\sigma}$ becomes ordered (corresponding to the nematic phase) and anisotropy is expected. S_0 is the Lebwohl-Lasher potential,

which is used for the study of the phase transition in LC between the nematic and isotropic phases. S_1 is the Gaussian bond potential, where the tension is fixed to $\gamma = 1$. S_1 is given by:

$$S_1 = \int \sqrt{g} d^3x g^{ab} \frac{\partial \vec{r}}{\partial x_a} \cdot \frac{\partial \vec{r}}{\partial x_b} \tag{2}$$

where $x_a (a = 1,2,3)$ is the parameter of the spherical body, and g^{ab} is the inverse of the Finsler metric g_{ab}:

$$g_{ab} = \begin{pmatrix} 1/v_{12}^2 & 0 & 0 \\ 0 & 1/v_{13}^2 & 0 \\ 0 & 0 & 1/v_{14}^2 \end{pmatrix}, \qquad v_{ij} = \left|\vec{\sigma}_i \cdot \vec{t}_{ij}\right|, \tag{3}$$

where g is the determinant, and $\vec{t}_{ij}$ is the unit vector of the bond ij along the direction $i \to j$ vertices such that $\vec{t}_{ij} = \left(\vec{r}_j - \vec{r}_i\right) \Big/ \left|\vec{r}_j - \vec{r}_i\right|$. The $\bar{N}$ in Eq. (1) given by $\bar{N} = (1/N_B) \sum_{ij} n_{ij}$, where N_B is the total number of the bonds, and n_{ij} is the total number of the tetrahedrons sharing the ij bond. The coefficients γ_{ij} in Γ_{ij} are defined by:

$$\begin{aligned} \gamma_{12} &= \frac{v_{12}}{v_{13}v_{14}} + \frac{v_{21}}{v_{23}v_{24}} \quad \gamma_{13} = \frac{v_{13}}{v_{12}v_{14}} + \frac{v_{31}}{v_{32}v_{34}}, \\ \gamma_{14} &= \frac{v_{14}}{v_{12}v_{13}} + \frac{v_{41}}{v_{43}v_{42}} \quad \gamma_{23} = \frac{v_{23}}{v_{21}v_{24}} + \frac{v_{32}}{v_{31}v_{34}}, \\ \gamma_{24} &= \frac{v_{24}}{v_{23}v_{21}} + \frac{v_{42}}{v_{41}v_{43}} \quad \gamma_{34} = \frac{v_{34}}{v_{31}v_{32}} + \frac{v_{43}}{v_{41}v_{42}}. \end{aligned} \tag{4}$$

Note that $\gamma_{ij} = \gamma_{ji}$ (see (Osari and Koibuchi, 2017) for the details). The κS_2 is the energy for maintaining the shape of tetrahedrons, where κ is the rigidity coefficient corresponding to the polymer stiffness. The ϕ_i is the internal angle of the triangles Fig.1(b). The αS_3 is the interaction energy between $\vec{\sigma}$ and the external electric field $\vec{E}$, where α corresponds to the dielectric anisotropy $\Delta\varepsilon$, which will be discussed later. The potential U_{3D} protects the tetrahedron volume from being negative.

The partition function is defined by:

$$Z = \sum_{\vec{\sigma}} \int \prod_{i=1}^{N} d\vec{r}_i \exp[-S(\vec{r}, \vec{\sigma})], \tag{5}$$

where $\Sigma_{\vec{\sigma}}$ denotes the sum of all possible values of $\vec{\sigma}$.

In the simulations, the volume V of the sphere is fixed to a constant value such as

$$V = V_0. \tag{6}$$

See (Osari and Koibuchi 2017) for the details on the volume constant simulation. The constant V_0 in Eq. (6) is determined in the simulations without the constraint of Eq. (6) using the same parameters as the volume constant simulations.

3. DETAILS OF EXISTING EXPERIMENTAL DATA

In this chapter, we would like to introduce the details of the existing experiment reported in (Urayama et al. 2005). The data in (Urayama et al. 2005) are used for the comparison with the simulation data. In this Urayama's paper, the authors experimentally studied electrically driven deformation of the side chain nematic LCE swollen by nematic solvent.

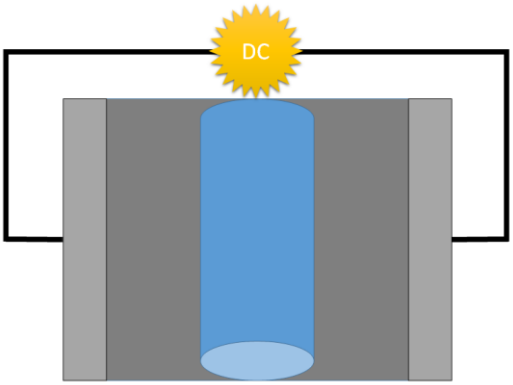


Fig. 2. Schematic representation of the experimental setup in (Urayama et al. 2005).

The samples are in the cylindrical shape. They are placed in the cell between electrodes (Fig.2). Also, the cell is filled with the nematic solvent. The temperature is controlled to change the phase states, nematic or isotropic, of the LCE and the surrounding solvent.

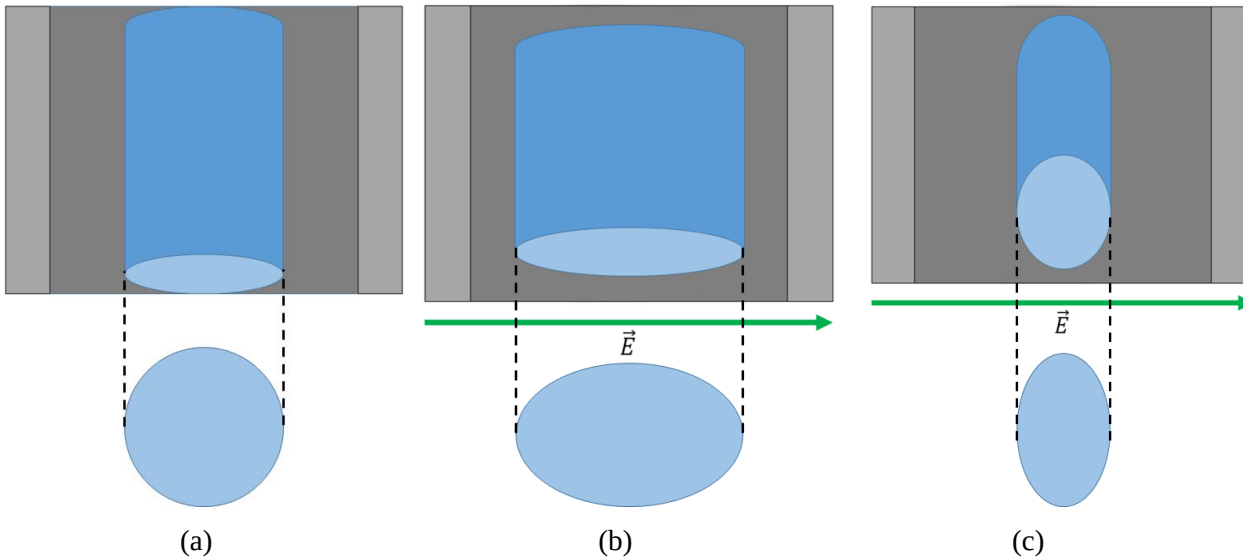


Fig. 3. The shape of samples (a) before and (b), (c) after applying external electric field E with positive (b) and negative (c) dielectric anisotropy.

When the dielectric anisotropy of the sample is positive, the sample is stretched in the field direction and compressed in the normal to the field axes (Fig.3(b)). In contrast, when the dielectric anisotropy is negative, the sample is compressed in the field direction and stretched in the normal to the field direction (Fig.3(c)).

Note that the volume of LCE under electric field remains unchanged after the elongation. The deformation behavior of LCE, which consist of the nematic network and solvent, depends on the sign of the dielectric anisotropy, on the phase state (nematic or isotropic), and on the elasticity. The sample deformation can also be influenced by the surrounding solvent, however, this influence can be neglected because the same solvents are used inside and outside.

However, the direction of the LC molecules in the initial state ($E = 0$) is unclear, because there is no noticeable variation in birefringence before and after applying electric field (Urayama et al. 2005). For this reason, we start with a random initial configuration for the LC molecules corresponding to the isotropic phase.

4. RESULTS

4.1. Monte Carlo simulation data

In the simulations, we use a sphere instead of a cylinder for simplicity. The Metropolis MC technique was used for update parameters $\vec{r}$ and $\vec{\sigma}$. First, we show the Monte Carlo data. The strain $^{L}/_{L_0} - 1$ vs. external field E, and the order parameter M vs. E for $\kappa = 0.3$, $\lambda = 0; 0.1; 0.2$ are plotted in Figs. 4(a) and 4(b). M is defined by:

$$M = \frac{3}{2}\left(\frac{1}{N}\sum_i \sigma_{iz}^2 - \frac{1}{3}\right) \tag{7}$$

where σ_{iz} is the z-component of σ_i (Koibuchi 2017).

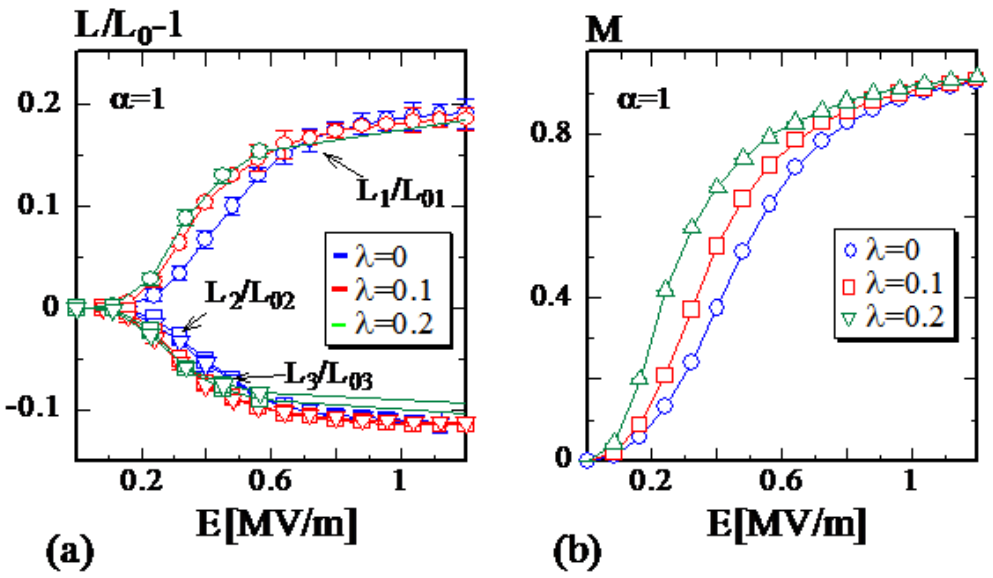


Fig. 4. Results of the model simulation for $N = 10619$. (a) The strain $^{L}/_{L_0} - 1$ vs. external field E for $\kappa = 0.3$, $\lambda = 0; 0.1; 0.2$, and (b) the order parameter M vs. E.

In the strains $^{L_i}/_{L_{0i}} - 1, (i = 1,2,3)$, L_{0i} $(i = 1,2,3)$ denote the initial $(E = 0)$ sizes of the sphere, and $L_i (i = 1,2,3), (L_1 > L_2 > L_3)$ are the final sizes of the sphere. Indices $i = 1,2,3$ correspond to the direction of the strain of the sphere as shown in the Fig.5.

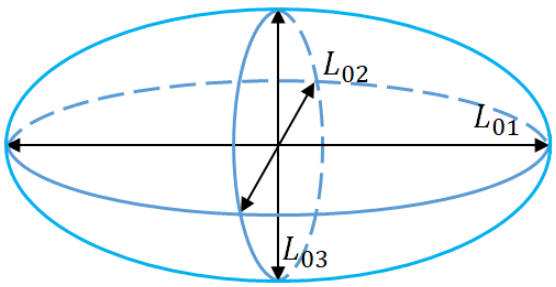


Fig. 5. Diameters L_{01}, L_{02}, L_{03} in a deformed sphere, where $L_{01} > L_{02} > L_{03}$

From Fig. 4 we can see how the strain and M depend on λ. The strain abruptly changes for the small region of E, and this change becomes sharp with increasing λ. This is because the interaction between σs is strengthened with increasing λ, and this means that the response of alignment of $\vec{\sigma}$ to the electric field becomes stronger for non-zero λ than the case of $\lambda = 0$. In this figure, the value of strain in the limit of $E \to \infty$ is independent of λ. It is not necessary to say that M in the limit of $E \to \infty$ is independent of λ (Figs.4(a),4(b)).

The results of $L/L_0 - 1$ and M are plotted in Fig.6, where κ is varied. We see that M is almost independent of κ. In contrast, $L/L_0 - 1$ is noticeably dependent on κ. Indeed, when κ is increased, the strain is decreased. This is reasonable, because the material is hard to deform for large κ.

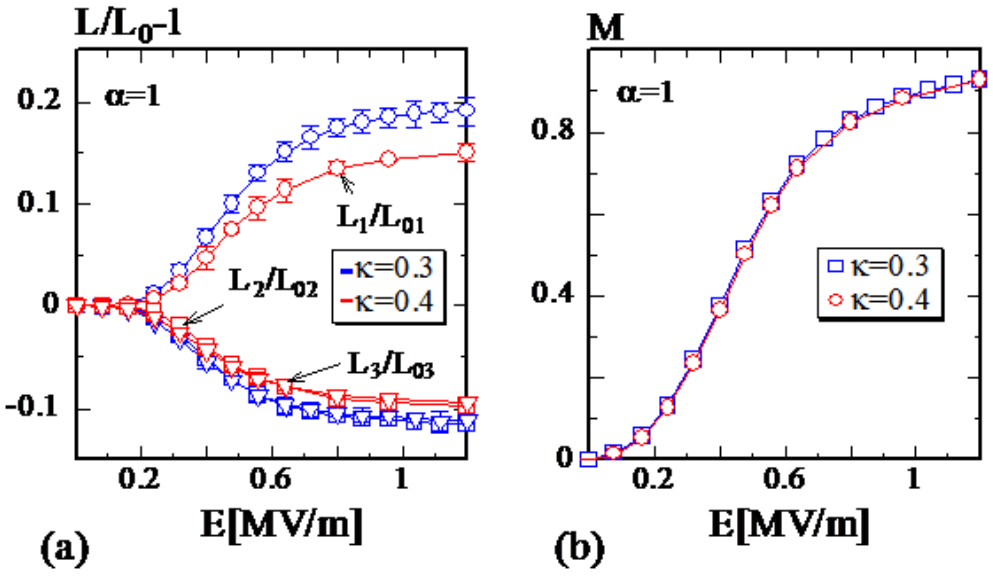
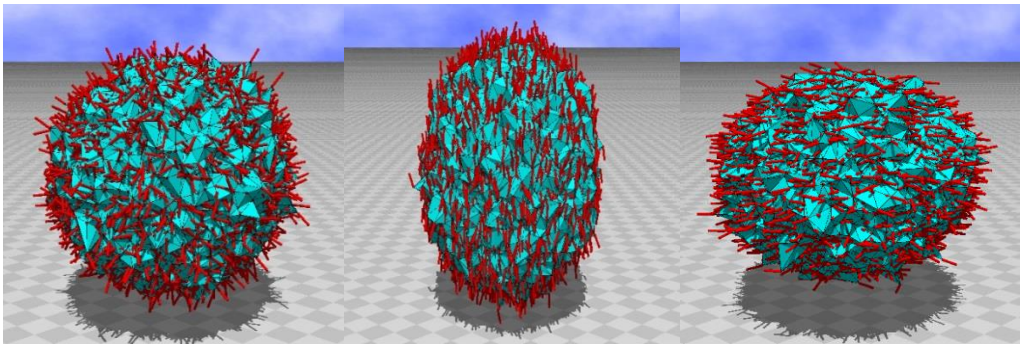


Fig. 6. Results of the simulation for $N = 10619$. (a) Strain $L/L_0 - 1$ vs. E for $\lambda = 0$, $\kappa = 0.3; 0.4$, (b) M vs. E.

4.2. Snapshots



(a) (b) (c)

Fig. 7. Snapshots of the spheres of size $N = 16124$, $\lambda = 0, \kappa = 0.3$, where the external field E is vertically applied. $E = 0$ in (a), and $E = 1.2$ in (b) $\alpha = 1$ and (c) $\alpha = -1$ corresponding to positive and negative dielectric anisotropy. The shape in (a) is symmetric under the rotation of any axes, while these in (b) and (c) are symmetric only around z axis.

First we show the snapshots of the spheres, of which the size is N=16124. We assume $\lambda = 0$ and $\kappa = 0.3$ with positive (Fig.7(b)) and negative (Fig.7(c)) dielectric anisotropy $\Delta\varepsilon = \varepsilon_{\parallel} - \varepsilon_{\perp}$, where $\varepsilon_{\parallel}$ and $\varepsilon_{\perp}$ are the dielectric constant along and perpendicular to the field direction (Urayama et al. 2005). In our model, we assume the following two cases:

$$\Delta\varepsilon > 0 \ \text{(positive)}, \quad \Delta\varepsilon < 0 \ \text{(negative)}. \tag{8}$$

Therefore, $\Delta\varepsilon > 0$ ($\Delta\varepsilon < 0$) corresponds to positive (negative) α in Eq. (1). The electric field is $E = 0$ (Fig.7(a)) and $E = 1.2$ (Fig.7(b),7(c)). When $E = 0$, the sphere remains unchanged and all LC molecules are at random because of the isotropic phase ($\lambda = 0$). When we increase E, the sphere shape changes. When the dielectric anisotropy is positive (negative), the sphere elongates in the electric field direction (orthogonal to the field direction) and shrinks into the orthogonal direction (the field direction) as we can see in Fig. 7(b) (Fig. 7(c)).

4.3. Comparison with the experimental data

Next we compare the numerical results of the FG model for $v_{ij} = \left|\vec{\sigma}_i \cdot \vec{t}_{ij}\right|$ with experimental data (Fig.8). To do this, we should pay attention to the unit of energy αS_3. In the simulation, the unit of αS_3 is assumed to be $[k_{\mathrm{B}}\mathrm{T}]$. On the other hand, in the experiment $\varepsilon_0\Delta\varepsilon\left(\vec{\sigma}_i \cdot \vec{E}\right)^2$ has the unit of $\left[\frac{\mathrm{N}}{\mathrm{m}^2}\right] = [\mathrm{Pa}]$. Therefore, to compare $\alpha\left(\vec{\sigma}_i \cdot \vec{E}_{\mathrm{sim}}\right)^2 k_{\mathrm{B}}T$ [Nm] with $\varepsilon_0\Delta\varepsilon\left(\vec{\sigma}_i \cdot \vec{E}\right)^2$[Pa], the simulation data $\alpha\left(\vec{\sigma}_i \cdot \vec{E}_{\mathrm{sim}}\right)^2 k_{\mathrm{B}}T$ [Nm] should be divided by a parameter that has the unit of [m^3]. What is this parameter? The answer is a^3, in which a[m] is the lattice spacing. The lattice spacing is always assumed to be $a = 1$ in the simulations for simplicity. Thus, we have

$$\alpha E_{\mathrm{sim}}^2 k_{\mathrm{B}}T \Big/ a^3 = \varepsilon_0\Delta\varepsilon E^2 \iff \alpha k_{\mathrm{B}}T \Big/ a^3 = 8.85\Delta\varepsilon. \tag{9}$$

The second equation is obtained with the condition $E_{\mathrm{sim}}^2 = 10^{-12}E^2$(see Fig. 8) and $\varepsilon_0 = 8.85 \times 10^{-12}$. This equation is satisfied for the given parameters α, T and $\Delta\varepsilon$ if we suitably choose a. Indeed, we have $a = 3.06 \times 10^{-8}$ for $\alpha = 1.37$, $k_{\mathrm{B}}T = 4 \times 10^{-21}$ and $\Delta\varepsilon = 11.5$ (Cummins, Dunmur and Laidler 1975) in the case of Fig. 8(a), and $a = 2.83 \times 10^{-8}$ for $\alpha = -4$, $k_{\mathrm{B}}T = 4 \times 10^{-21}$ and $\Delta\varepsilon = -5$ in the case of Fig. 8(b), where the negative $\Delta\varepsilon$ is unknown (Urayama et al. 2005), and hence we assume $\Delta\varepsilon = -5$ for simplicity. The important point to note is that these parameter changes can be absorbed into the free parameter a. Only constraint is that a should be smaller than the Van der Waals distance between atoms, and therefore we find that these obtained a are reasonable as the lattice spacing.

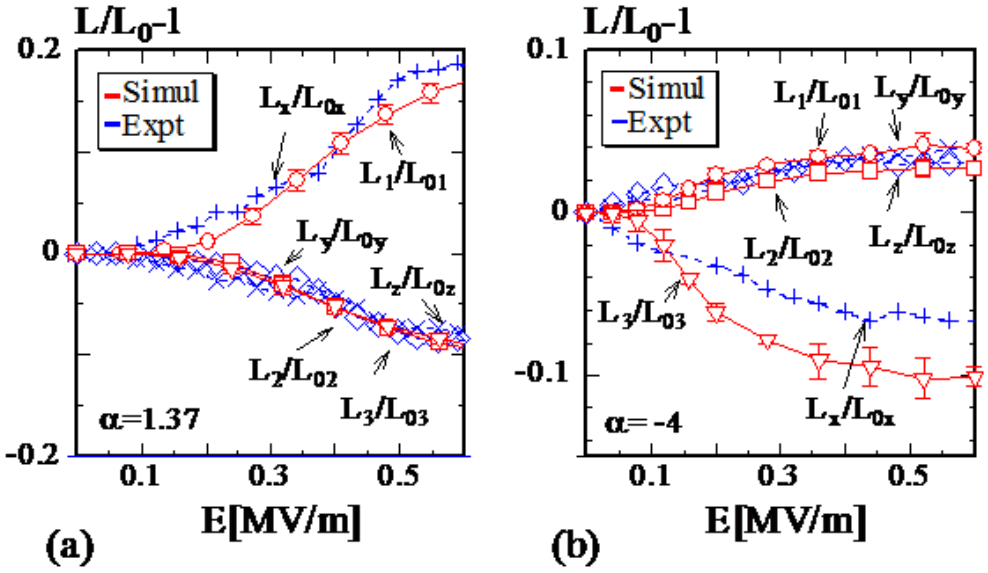


Fig. 8. Comparison of the simulation and experimental data of LCE elongation under electric field. The simulation parameters are $\lambda = 0$, $\kappa = 0.3$ for $N = 10619$. The dielectric anisotropy is positive in (a) $\alpha = 1.37$, and negative in (b) $\alpha = -4$.

The simulation and experimental data $^{L}/_{L_0} - 1$ versus external electric field E are plotted in Fig.8 for positive (a), and negative (b) dielectric anisotropy. The meaning of the data symbols is the same for both cases. For positive anisotropy, we use $\lambda = 0$, $\kappa = 0.3$ parameters, and for negative $\lambda = 0.1$, $\kappa = 0.3$.

For the simulations, we assume $\lambda = 0; 0.1$. This is because the variable σ is at random for $\lambda = 0; 0.1$, and therefore the sphere remains unchanged for $E = 0$, and the simulation results $E \geq 0$ are expected to be independent of the initial configuration. For the nematic phase the sphere becomes oblong even when $E = 0$, and therefore the simulation results for $E \geq 0$ are expected to be dependent on the initial configuration. For this reason, we use these values $\lambda = 0; 0.1$ corresponding to the isotropic phase.

For positive dielectric case (Fig.8(a)), we find that the simulation data are in good agreement with the experimental data. As we can see in Fig.8(b), for the negative dielectric case, the value of the strain $^{L_3}/_{L_0} - 1$ is slightly different from the experimental data. The origin of the difference is unclear at present, however, this will be clarified in the future studies.

5. CONCLUSION

We have studied the elongation phenomenon of the LCE under an external electric field using FG model. We assume the nonpolar interaction between $\vec{\sigma}$ and $\vec{E}$ and between $\vec{\sigma}$s. We use two different Finsler metrics and compare our results with the experimental data reported in (Urayama et al. 2005). From the simulation data, we find that the simulation data are almost in good agreement with the existing experimental data. Our numerical data support that the FG modeling in (Koibuchi and Sekino 2014; Osari and Koibuchi 2017) well describes the anisotropic shape transformation under external electric field.

The remaining tasks are to clarify whether the FG model in the nematic states describes the experimental data or not. In the numerical simulations in this paper, we use sphere, which is not always identical to the shape (=cylinder) of LCE in the experiment in (Urayama et al. 2005). Therefore, it is also interesting to use cylinder in the numerical simulations. The FG modeling is also

expected to be possible for other objects such as ferroelectric polymer films, in which the shape also depends on the polymer orientation.

ACKNOWLEDGEMENT

This work is supported in part by JSPS KAKENHI No. 17K05149.

REFERENCES

Cummins, P., Dunmur, D. and Laidler, D. (1975). Dielectric properties of nematic 4,4'-n-pentylcyanobiphenyl. *Molecular Crystals and Liquid Crystals*, 30(1-2), pp.109-123.

de Gennes PG (1975) One type of nematic polymers. Comptes Rendus Hebdomadaires Des Seances De L Academie Des Sciences Serie B 281(5-8): pp.101-103

de Gennes, P., Hébert, M. and Kant, R. (1997). Artificial muscles based on nematic gels. *Macromolecular Symposia*, 113(1), pp.39-49.

Koibuchi, H. (2017). Finsler geometry modeling of elongation of flexible materials under external electromagnetic field. Ferroelectrics, 508(1), pp.144-150.

Koibuchi, H. and Sekino, H. (2014). Monte Carlo studies of a Finsler geometric surface model. *Physica A: Statistical Mechanics and its Applications*, 393, pp.37-50.

Madden, J., Vandesteeg, N., Anquetil, P., Madden, P., Takshi, A., Pytel, R., Lafontaine, S., Wieringa, P. and Hunter, I. (2004). Artificial Muscle Technology: Physical Principles and Naval Prospects. IEEE Journal of Oceanic Engineering, 29(3), pp.706-728.

Matsumoto, M. (1975). *Keiryou Bibun Kikagaku* (in Japanese), 1st ed. Tokyo: Shokabo.

Ohm, C., Brehmer, M. and Zentel, R. (2010). Liquid Crystalline Elastomers as Actuators and Sensors. *Advanced Materials*, 22(31), pp.3366-3387.

Osari, K. and Koibuchi, H. (2017). Finsler geometry modeling and Monte Carlo study of 3D liquid crystal elastomer. *Polymer*, 114, pp.355-369.

Sánchez-Ferrer, A. (2014). Liquid crystal elastomers: materials and applications, by W.H. de Jeu. *Liquid Crystals Today*, 23(2), pp.44-45.

Urayama, K. (2007). Selected Issues in Liquid Crystal Elastomers and Gels. *Macromolecules*, 40(7), pp.2277-2288.

Urayama, K. (2011). Electro-Opto-Mechanical Effects in Swollen Nematic Elastomers. *Advances in Polymer Science*, 250, pp.119-145.

Urayama, K., Kondo, H., Arai, Y. and Takigawa, T. (2005). Electrically driven deformations of nematic gels. *Physical Review E*, 71(5).

Warner, M. and Terentjev, E. (2003). *Liquid crystal elastomers*. 1st ed. Oxford: Oxford University Press.